Biophysical Journal
Article

Biophysical Society

Mechanics and Dynamics of Bacterial Cell Lysis

Felix Wong[1] and Ariel Amir[1,*]
[1]John A. Paulson School of Engineering and Applied Sciences, Harvard University, Cambridge, Massachusetts

ABSTRACT Membrane lysis, or rupture, is a cell death pathway in bacteria frequently caused by cell wall-targeting antibiotics. Although previous studies have clarified the biochemical mechanisms of antibiotic action, a physical understanding of the processes leading to lysis remains lacking. Here, we analyze the dynamics of membrane bulging and lysis in *Escherichia coli*, in which the formation of an initial, partially subtended spherical bulge ("bulging") after cell wall digestion occurs on a characteristic timescale of 1 s and the growth of the bulge ("swelling") occurs on a slower characteristic timescale of 100 s. We show that bulging can be energetically favorable due to the relaxation of the entropic and stretching energies of the inner membrane, cell wall, and outer membrane and that the experimentally observed timescales are consistent with model predictions. We then show that swelling is mediated by the enlargement of wall defects, after which cell lysis is consistent with both the inner and outer membranes exceeding characteristic estimates of the yield areal strains of biological membranes. These results contrast biological membrane physics and the physics of thin, rigid shells. They also have implications for cellular morphogenesis and antibiotic discovery across different species of bacteria.

INTRODUCTION

Antibiotic resistance is one of the largest threats to global health, food security, and development today (1). Its increasing prevalence (2) begs the question of whether physical principles, which may be more universal than particular chemical pathways, could inform work on novel therapeutics as has been done for mechanotransduction in eukaryotes (3) and tissue growth and fluidity (4,5). To elucidate such principles, a physical understanding of the cell death pathway caused by many antibiotics, which may complement the knowledge of related biochemical mechanisms (6–12), is needed.

In many bacteria, cell shape is conferred by the cell wall, which resists the internal turgor pressure and is composed of two- or three-dimensional layers of peptidoglycan (PG) (13–15). In Gram-negative bacteria such as *Escherichia coli*, the two-dimensional cell wall is sandwiched between the inner membrane (IM) and outer membrane (OM), whereas in Gram-positive species, the cellular envelope comprises an IM enclosed by a three-dimensional cell wall. PG consists of rigid glycan strands cross-linked by peptide bonds and is maintained through the combined, synchronized activity of enzymes, including transglycosylases and transpeptidases (13,15–17). Many antibiotics, such as β-lactams, bind to transpeptidases to inhibit cross-linking. Inhibition of peptide bond formation and cell wall synthesis results in large defects in the cell wall, which precede bulging of the IM and OM and eventual cell lysis (6,7,18–20).

In this work, we show how the response of the bacterial cell envelope to large, micron-scale defects in the cell wall can be modeled physically. By dissecting the dynamics of lysis, we reveal salient features—the emergence of different timescales and the formation of partially subtended, spherical bulges—that require explanation. We then show that a theoretical model comprising turgor pressure and cell envelope stretching is consistent with these features. By clarifying aspects of membrane physics, entropy, and water flow, the model illustrates how lysis arises as a generic, mechanical response and how different cell envelope components interact during bulging. We anticipate these results to be useful for revealing a better understanding of antibiotic action, probing lysis in other experimental contexts, and modeling related systems involving biological membranes and elastic shells, as discussed further in the Conclusions.

MATERIALS AND METHODS

Model parameters

We briefly discuss the choice of parameter values in this work here, with further details provided below and in Table 1. We model the cell wall as a rigid, orthotropic cylindrical shell with elastic moduli $Y_x^w = 0.1$ N/m

Submitted July 16, 2018, and accepted for publication April 25, 2019.
*Correspondence: arielamir@seas.harvard.edu
Editor: Amy Palmer.
https://doi.org/10.1016/j.bpj.2019.04.040

TABLE 1 Variables Used, or Calculated, in This Work for *E. coli* and Their Estimated Numerical Ranges

Quantity	Estimate	Source
Axial cell wall elastic modulus (3D), E_x^w	20–30 MPa	(21–23).
Circumferential cell wall elastic modulus (3D), E_y^w	50–75 MPa	(21,24).
Cell wall thickness, h^w	3–4 nm	(23,70).
Axial cell wall elastic modulus (2D), Y_x^w	0.06–0.12 N/m	$Y = Eh$
Circumferential cell wall elastic modulus (2D), Y_y^w	0.15–0.30 N/m	$Y = Eh$
Cell wall Poisson's ratio, ν_{xy}^w	0.2	(23).
Cell wall Poisson's ratio, ν_{yx}^w	0.25–1	$\nu_{yx}^w = Y_y^w \nu_{xy}^w / Y_x^w$
Cell membrane area stretch modulus, K_a	0.03–0.24 N/m	(25).
Turgor pressure, p	0.3–2 atm	(21,71,72).
Number of solute molecules, n_s	$(5.7 - 38) \times 10^7$ molecules	$p \approx kTn_s/[\pi(r_0^w)^2 L_0^w]$
Reference cell wall radius, r_0^w	0.5 μm	–
Reference cell wall length, L_0^w	10 μm	–
Reference cell wall surface area, $\mathcal{A}^w$	31.4 μm^2	$\mathcal{A}^w = 2\pi r_0^w L_0^w$
Reference membrane surface area ratio, $\gamma = \mathcal{A}^i/\mathcal{A}^w$	1.0–1.2	this work
Membrane bending modulus, k_b	10–20 kT	(27).
Temperature, T	300 K	–

2D, two-dimensional; 3D, three-dimensional.

(axial direction, x) and $Y_y^w = 0.2$ N/m (circumferential direction, y) (21–24). The Poisson's ratios are $\nu_{xy}^w = 0.2$ and $\nu_{yx}^w = 0.4$ (23), the reference cell wall radius is $r_0^w = 0.5$ μm, the reference cell wall length is $L_0^w = 10$ μm, and the reference cell wall area, neglecting the cellular poles, is $\mathcal{A}^w = 2\pi r_0^w L_0^w$. The area stretch moduli of both the IM and OM are set to $K_a^i = K_a^o = 0.1$ N/m (25–27); here and below, we use superscripts to denote IM (i), OM (o), or cell wall (w) quantities. The membrane bending rigidity is $k_b^i = k_b^o = 20\,kT$, where k denotes Boltzmann's constant and $T = 300$ K is the temperature (27). The number of solute molecules inside the cell is taken to be $n_s = 9.5 \times 10^7$, corresponding approximately to a turgor pressure of $p = 0.5$ atm for the cellular dimensions considered in this work (21). To contextualize the choice of parameter values above, Table 1 provides estimated ranges of all parameter values found in the literature.

Bacterial strains and microscopy

The wild-type strain used in this study is *E. coli* MG1655, and we verified that the morphological dynamics is statistically indistinguishable in two other wild-type strains, JOE309 and BW25113. The Supporting Materials and Methods contains further details regarding bacterial growth, microscopy, and image analysis.

RESULTS AND DISCUSSION

Dynamics of bacterial cell lysis

Inspired by previous work (16), we degraded wild-type *E. coli* cell walls with cephalexin, a β-lactam antibiotic, at a concentration of 50 μg/mL and observed typical cells to undergo the morphological transitions shown in Fig. 1, *A–C* and Video S1. Bulging—defined here as the development of an initial protrusion, which may be accompanied by a noticeable shrinking of the cell length—was observed to occur as fast as 100 ms (16) but on a typical timescale of 1 s. Swelling, defined here as the growth of the protrusion, was observed to occur on a typical timescale of 100 s (Fig. 1 *D*).

In a recent modeling study (28), a critical cell wall pore size for bulging was found by studying the trade-off between the bending energy cost of bulging and the pressure-volume energy gained. This trade-off appears to be irrelevant for determining bulge size in our experiments, in which it can be shown that the bending energies are negligible compared to the stretching energies, as discussed below. As we shall see, membrane remodeling and the relaxation of the entropic and stretching energies of the cell envelope can predict bulging and are consistent with the separation of timescales shown in Fig. 1 *D*.

Cell envelope mechanics

We model the cell wall, IM, and OM as linear-elastic shells. Importantly, we suppose that, on timescales comparable to that of bulging, the membrane geometries can vary because of membrane fluidity while conserving their reference surface areas. This contrasts the IM and OM with the rigid cell wall, whose reference configuration is assumed to be a cylinder. The free energy of the cell wall, IM, OM, and the volume enclosed by the IM is as follows:

$$\mathcal{F} = E_{\text{stretch}}^w + E_{\text{stretch}}^i + E_{\text{stretch}}^o + E_{\text{bend}}^w + E_{\text{bend}}^i + E_{\text{bend}}^o - TS, \quad (1)$$

where the superscripts ^{w}, ^{i}, and ^{o} denote wall, IM, and OM quantities, respectively; E_{stretch} and E_{bend} are the stretching and bending energies, respectively, of an elastic shell; T is the temperature; and S is the entropy of mixing water and solutes corresponding to the turgor pressure. Here, only water molecules are assumed to be outside the cell, the solute molecules are assumed to be enclosed by the IM, and $S = -k(n_s \ln x_s + n_w \ln x_w)$, where k is Boltzmann's constant, x_s and x_w are the number fractions of solute and water molecules inside the IM, respectively, and n_s and n_w are the numbers of solute and water molecules, respectively. Whereas we will assume n_s to be fixed (as discussed below), n_w depends on the volume,

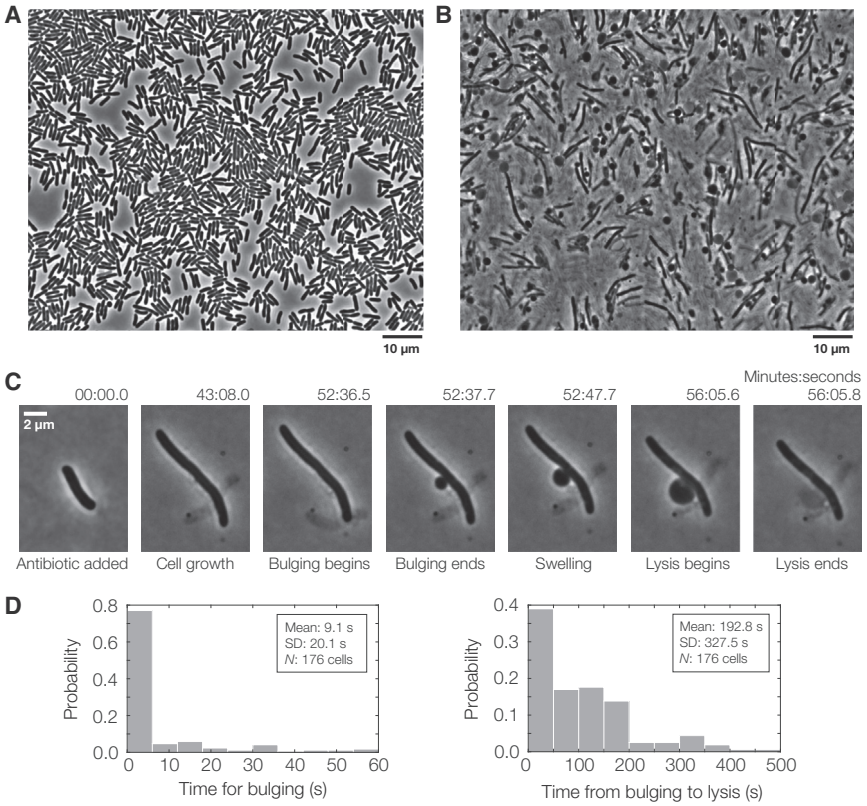

FIGURE 1 Experimental observation of membrane bulging, swelling, and lysis. (*A*) Shown is a phase-contrast image of a population of *E. coli* cells immediately after antibiotic treatment (see also Video S1). (*B*) A phase-contrast image of the same population ~1 h after antibiotic treatment shows that membrane bulging and swelling are common to most cells. (*C*) Shown is a phase-contrast time lapse of a single *E. coli* cell during antibiotic killing, with the corresponding stages of lysis denoted. (*D*) Histograms of the time for bulging and the time between bulging and lysis illustrate the separation of timescales involved. The population mean, standard deviation (SD), and cell number (*N*) are indicated.

V^i, enclosed by the IM as $n_w = V^i/m_w$, where m_w is the volume occupied per water molecule. We also assume the solution to be ideal and dilute: while we assume $n_s = 9.5 \times 10^7$ molecules for a typical cell of the dimensions considered here, $n_w \approx 2.6 \times 10^{11}$ molecules and $n_s/n_w \sim 10^{-4}$.

Because the cell wall, IM, and OM are thin, it is convenient to simplify the stretching energies by integrating over the thicknesses and working with stress resultants. In particular, for the cell wall, the planar Young's moduli can be expressed in units of force per length. Building on evidence for a larger elastic modulus in the circumferential direction than the axial direction (21,24), we assume an orthotropic constitutive relation for the cell wall, so that $\sigma^w_{xx} = Y^w_x(u^w_{xx} + \nu^w_{yx}u^w_{yy})/(1 - \nu^w_{xy}\nu^w_{yx})$ and $\sigma^w_{yy} = Y^w_y(u^w_{yy} + \nu^w_{xy}u^w_{xx})/(1 - \nu^w_{xy}\nu^w_{yx})$. Here and below, $(Y^w_x, Y^w_y, \nu^w_{xy}, \nu^w_{yx})$ are the two-dimensional Young's moduli and Poisson's ratios of the cell wall. $(\sigma^\alpha_{xx}, \sigma^\alpha_{yy})$ denote in-plane stresses (or strains, u) in the axial and circumferential directions, respectively, of the α component of the cellular envelope ($\alpha \in \{i, o, w\}$); in general, we will also use x and y to denote orthogonal directions for geometries that are not cylindrical. E^w_{stretch} can then be expressed as

$$E^w_{\text{stretch}} = \frac{1}{2}\int \frac{\left(\sigma^w_{xx}\right)^2}{Y^w_x} + \frac{\left(\sigma^w_{yy}\right)^2}{Y^w_y} - \left(\frac{\nu^w_{xy}}{Y^w_x} + \frac{\nu^w_{yx}}{Y^w_y}\right)\sigma^w_{xx}\sigma^w_{yy}dA^w, \tag{2}$$

where dA is an area element in the deformed state. Unlike the rigid cell wall, the IM and OM are fluid and possess different stretching energies. Consistent with the fact that fluid membranes cannot support in-plane shears (29), we take the membrane shear moduli to be zero, so that the membrane stretching energies comprise of areal penalties alone,

$$E^\alpha_{\text{stretch}} = \frac{K^\alpha_a}{2}\int\left(u^\alpha_{xx} + u^\alpha_{yy}\right)^2 dA^\alpha = \frac{K^\alpha_a}{2}\int\left(\frac{\Delta A^\alpha}{A^\alpha}\right)^2 dA^\alpha, \tag{3}$$

where α ranges over $\{i, o\}$, $\Delta A/A$ is the fractional change in membrane area, and the equality holds because here and below, we assume a linear theory in which higher-order terms in the strains are neglected. For a vanishing shear modulus, K^α_a is equivalent to the first Lamé coefficient in two-dimensional elasticity (30,31). Values of K_a have been estimated to be in the range of $K_a \approx 0.03$–0.24 N/m for *E. coli* spheroplasts depending on the external osmolarity and size (25) and $K_a \approx 0.2$–0.4 N/m for red blood cells (RBCs) and giant unilamellar vesicles (27,32), and these values are expected to be similar for the IM and OM (25). As shown below, these values imply that the IM and OM can be as load bearing as the cell wall. Finally, for characteristic parameter values, the bending energies of Eq. 1 are negligible compared to the stretching energies, which

is usually the case for thin shells (33–35): whereas the bending energies scale as the third power of thickness, the stretching energies are linear in thickness. We therefore discard the bending energies in the expressions below and verify in the Supporting Materials and Methods that they do not change our results.

Homogeneity of membrane stresses

Before modeling the mechanics of lysis further, it is convenient to note a few properties of membrane stresses. As the reference membrane dimensions are allowed to vary because of fluidity, the strains u_{xx} and u_{yy} may vary. The stretching energy of Eq. 3 depends only on the trace of the membrane strain tensor, $\Delta A/A = u_{xx} + u_{yy}$. Hence, manifesting the fluid nature of the membranes, mathematically minimizing Eq. 1 over the reference membrane dimensions shows that $u_{xx} = u_{yy}$ at equilibrium. Let us write $g(x,y) = u_{xx} = u_{yy}$ to denote the strains as a function of general surface coordinates, (x,y), and note that, in a linear theory, the area element of the deformed geometry is related to that of the reference geometry by $dA_{\text{reference}} = (1 - 2g(x,y))dA_{\text{deformed}}$. Consider now the free energy expression of Eq. 1 and suppose that the cell envelope is in a state of equilibrium in which the reference membrane area constraint applies. As E^w_{stretch} and $-TS$ do not depend on the reference membrane dimensions, the minimization of $\mathcal{F}$ in Eq. 1 is equivalent to the following:

$$\min_{g(x,y)} \int g(x,y)^2 dxdy, \tag{4}$$

subject to the constraint of a fixed membrane reference area,

$$\mathcal{A} = \int (1 - 2g(x,y))dxdy, \tag{5}$$

where $\mathcal{A}$ is a constant membrane reference area. Minimizing the functional of Eq. 4 under the constraint of Eq. 5 shows that $g(x,y)$ is constant. Thus, regardless of the deformed geometry, the membrane stresses are not only isotropic (36,37) but also spatially homogeneous at equilibrium. As we will assume the IM and OM to have identical material properties and reference areas, the same argument applies for both the IM and OM and shows that the stresses in these two layers are everywhere identical. Intriguingly, the membrane stresses in other contexts, such as the junctions of epithelial cells and eukaryotic cell blebs, have also been suggested to be spatially uniform (38–40).

The homogeneity of the membrane stresses places constraints on the bulged geometries considered below. In particular, at equilibrium and without the cell wall, the stresses $\sigma_{xx} = \sigma_{yy} = K_a(u_{xx} + u_{yy})$ in a membrane are anticipated to satisfy Laplace's law,

$$\frac{\sigma_{xx}}{\kappa_x} + \frac{\sigma_{yy}}{\kappa_y} = p, \tag{6}$$

where x and y are two principal directions, κ_x and κ_y are the two principal radii of curvature, and p is the turgor pressure. As the stresses are both isotropic and spatially homogeneous, we find that the equilibrium shapes of the membranes possess constant mean curvature. We will use this fact to constrain the shapes of the bulges we consider below as spherical caps.

The healthy state

To model the mechanics of lysis, the type of calculation we undertake below with Eq. 1 will be as follows. We ignore the cellular poles for simplicity and assume the reference surface area of the IM (and OM), $\mathcal{A}^i$ ($\mathcal{A}^o$), and the reference radius r^w_0 and length L^w_0 of the cell wall to be given. As the cell wall is rigid, we suppose that the membranes assume the shape of the cell wall, so that their deformed geometries are cylinders with radii and lengths (r^i,r^o) and (L^i,L^o), respectively. This assumption will be supported by the numerical calculations below, which show that the membranes are in contact with the cell wall. Given the material properties of the cell envelope, $\mathcal{A}^i$, $\mathcal{A}^o$, r^w_0, and L^w_0, we minimize $\mathcal{F}$ over 1) the deformed cylindrical cell wall dimensions, r^w and L^w, 2) the deformed cylindrical membrane dimensions, (r^i,r^o) and (L^i,L^o), and 3) the reference membrane cylindrical dimensions, (r^i_0, r^o_0) and (L^i_0, L^o_0), which satisfy the constraints $2\pi r^i_0 L^i_0 \leq \mathcal{A}^i$ and $2\pi r^o_0 L^o_0 \leq \mathcal{A}^o$. The inequalities in these constraints allow for membrane invaginations and less membrane surface area to be stretched than is available. Because of steric exclusion, we further require $r^i \leq r^w \leq r^o$ and $L^i \leq L^w \leq L^o$. The 10 foregoing variables and the linear strain-displacement relations $u_{xx} = (L - L_0)/L_0$, $u_{yy} = (r - r_0)/r_0$ then entirely determine F. To summarize,

$$\mathcal{F}_e = \min_{r^w,L^w,r^i,L^i,r^o,L^o,r^i_0,L^i_0,r^o_0,L^o_0} \mathcal{F} \text{ subject to } \quad 2\pi r^i_0 L^i_0 \leq \mathcal{A}^i, \\ 2\pi r^o_0 L^o_0 \leq \mathcal{A}^o, r^i \leq r^w \leq r^o, L^i \leq L^w \leq L^o \tag{7}$$

describes the equilibrium conformation of a healthy, intact cell.

To simplify the analysis further, we assume the IM and OM to share the same reference area for the remainder of this work, so that $\mathcal{A}^i = \mathcal{A}^o$ and all equations involving the OM are identical to their counterparts for the IM. We now solve for the equilibrium state both analytically and numerically, the former by determining the stresses using Laplace's law and the reference area constraint and the latter by undertaking the minimization in Eq. 7 explicitly. For the former, we start by assuming $r = r^w = r^i = r^o$ and

$L = L^w = L^i = L^o$, so that the envelope layers are in contact, and suppose the membrane reference area to be limiting, so that $2\pi r_0^i L_0^i = \mathcal{A}^i$. As the membrane stresses are isotropic and homogeneous at equilibrium, we set $\sigma = \sigma_{xx}^i = \sigma_{yy}^i = \sigma_{xx}^o = \sigma_{yy}^o$. It then follows from Laplace's law that

$$\frac{pr}{2} = \sigma_{xx}^w + 2\sigma, \quad pr = \sigma_{yy}^w + 2\sigma, \tag{8}$$

where $p = kTn_s/(\pi(r_0^w)^2 L_0^w(1 + u_{xx}^w + 2u_{yy}^w))$, and henceforth, all equalities will be accurate to the first order in the strains. Substituting the linear strain-displacement relations for the cell wall and solving for L and r, we find two simple expressions,

$$L = L_0^w - \frac{kTn_s\left(2Y_x^w\nu_{yx}^w - Y_y^w\right)}{2\pi r_0^w Y_x^w Y_y^w} + 2\sigma L_0^w\left(\frac{Y_x^w\nu_{yx}^w - Y_y^w}{Y_x^w Y_y^w}\right),$$
$$r = r_0^w + \frac{kTn_s\left(2Y_x^w - \nu_{xy}^w Y_y^w\right)}{2\pi L_0^w Y_x^w Y_y^w} + 2\sigma r_0^w\left(\frac{Y_y^w\nu_{xy}^w - Y_x^w}{Y_x^w Y_y^w}\right). \tag{9}$$

It remains to determine σ using the reference area constraint. As $u_{xx} = u_{yy} = \sigma/(2K_a)$ at equilibrium, the reference area constraint can be expressed as follows:

$$\mathcal{A}^i = 2\pi rL\left(1 - \frac{\sigma}{K_a}\right). \tag{10}$$

Substituting Eq. 9 into Eq. 10 yields a single equation in σ, for which the solution is as follows:

$$\sigma = \frac{K_a\left(-\left(\mathcal{A}^i - 2\pi r_0^w L_0^w\right)Y_x^w Y_y^w + kTn_s\left(2Y_x^w\left(1 - \nu_{yx}^w\right) + Y_y^w\left(1 - \nu_{xy}^w\right)\right)\right)}{2\pi r_0^w L_0^w\left(2K_a\left(Y_x\left(1 - \nu_{yx}^w\right) + Y_y\left(1 - \nu_{xy}^w\right)\right) + Y_x^w Y_y^w\right)}; \tag{11}$$

in turn, this solution determines all quantities of the equilibrium state. Building on evidence of finite excess membrane area in *E. coli* (25,41), we plot the predicted value of σ in Eq. 11 against $\mathcal{A}^i$ in Fig. 2 *A* for the parameter values summarized in Materials and Methods and note that, when $\gamma = \mathcal{A}^i/\mathcal{A}^w \approx 1$, the membrane stresses are nonzero and decreasing in γ. For the parameter values considered in this work, this occurs until $\gamma \approx 1.15$, at which point the equality in Eq. 10 is no longer valid—only the cell wall deforms—and the membrane stresses become zero. That the membrane stresses can be nonzero for smaller γ contrasts with the idea that the cell wall is the only load-bearing structure of the cellular envelope and is consistent with experimental observations suggesting that the IM and OM can also be load bearing, as manifested by the known fact that bulging precedes lysis (16). As the IM and OM are fluid, load bearing by the IM and OM does not contradict the fact that *E. coli* cells become spherical without their cell walls (42–44).

To verify the foregoing calculations, we numerically minimized Eq. 7 for the parameter values summarized in Materials and Methods and different values of $\mathcal{A}^i$ starting from $\gamma = 1.0$. We found that $\mathcal{F}$ is minimal when $2\pi r_0^i L_0^i, 2\pi r_0^o L_0^o = \mathcal{A}^i$ and $r^w = r^i = r^o \approx 0.53\ \mu$m, $L^w = L^i = L^o \approx 9.9\ \mu$m, $r_0^i = r_0^o \approx 0.52\ \mu$m, and $L_0^i = L_0^o \approx 9.7\ \mu$m. In this case, all envelope components are in contact and the stresses are $\sigma_{xx}^w \approx 1.5$ mN/m, $\sigma_{yy}^w \approx 12.6$ mN/m, and $\sigma_{xx}^i = \sigma_{xx}^o = \sigma_{yy}^i = \sigma_{yy}^o = K_a(u_{xx}^i + u_{yy}^i) = K_a(u_{xx}^o + u_{yy}^o) \approx 4.8$ mN/m, in good agreement with the linear theory (Fig. 2 *B*; Table S1). We then repeated the foregoing calculations across a range of larger reference surface areas $\mathcal{A}^i$. We found similar results in all cases, with the membrane stresses being generally dependent on $\mathcal{A}^i$ and decreasing in agreement with the linear theory (Fig. 2 *C*; Table S1). Below, we will also show that our prediction of bulging holds over a range of $\mathcal{A}^i$.

The bulged state

We now show that the removal of a piece of cell wall can result in bulging. Assuming that the membrane reference surface areas remain unchanged over the timescale of bulging, we consider a quasiequilibrium state in which they limit bulging. In contrast to the membrane areas, we do not assume cell volume to be limiting; as discussed below, characteristic timescales of water flow are fast in comparison to bulging. Since osmoregulation is believed to occur on a timescale of ~1 min for osmotic shocks applied over less than 1 s (45–47), we also assume the number of solute molecules to remain constant. The free energy may be lowered by water flow and bulging if the IM and OM may assume arbitrary geometries. Hence, we wish to minimize $\mathcal{F}$ over the cell geometry and the cellular dimensions, assuming that the membrane reference surface areas are fixed.

As mentioned above, when $\mathcal{F}$ is minimized, net flow of water into the cytoplasm may be required. The bulk flow of water from the external milieu to the cytoplasm is thought to be characterized by the hydraulic conductivity, L_p (48), defined so that the instantaneous volumetric flow rate through a membrane is $dV/dt = L_p A_{tot} \Delta P$, where A_{tot} is the total (strained) membrane surface area and ΔP is the

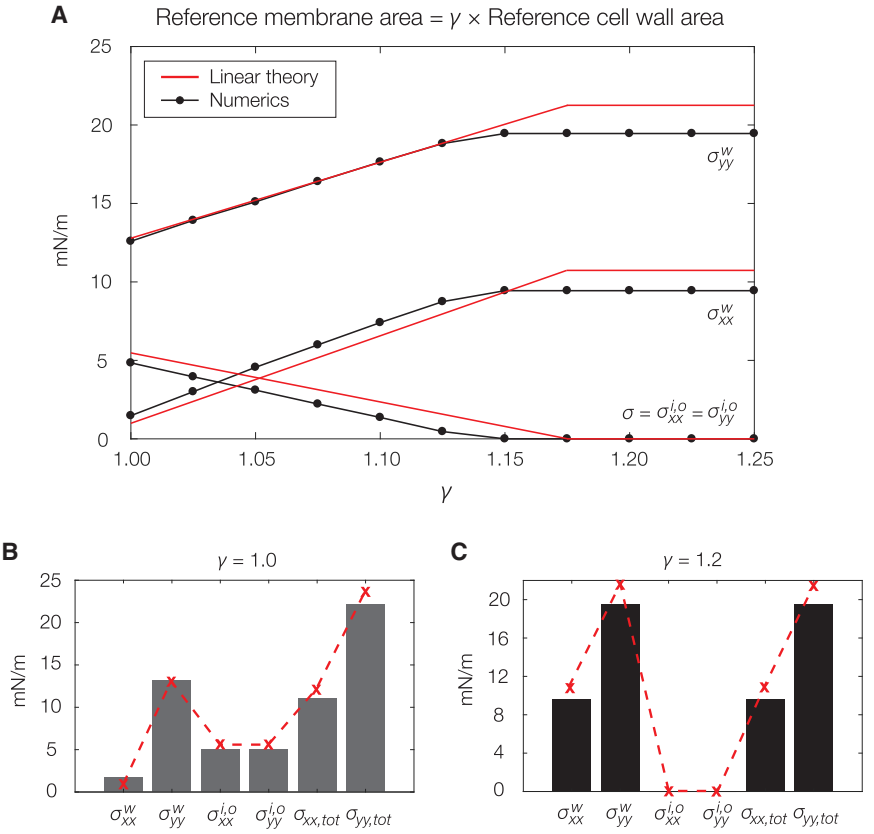

FIGURE 2 Stresses in the cellular envelope. (*A*) Shown are the stresses for the cell wall (*w*) and inner and outer membranes (*i* and *o*) as functions of the reference membrane area ratio, γ, with both the linear theory predictions (Eqs. 8 and 11) and independent numerical results plotted. The inner and outer membranes are assumed to share identical material properties and exhibit identical stresses. (*B* and *C*) Shown is the bar plot representation of two points in (*A*), as well as the stresses across the entire cell envelope (*tot*). The dashed lines indicate the linear theory predictions (Eqs. 8 and 11), whereas the bars indicate numerical results. To see this figure in color, go online.

pressure difference across the membrane, hereafter taken to be the turgor pressure p (45,48). Estimates of L_p vary depending on membrane structure; studies involving osmotically shocked bacteria (49), liposomes with aquaporin-1, and RBCs have found $L_p \approx 10^{-12}$ m^3/N·s, whereas studies for liposomes and other bilayers without water channels have indicated $L_p \approx 10^{-13}$ m^3/N·s (48,50). The larger value of L_p predicts a volume increase of ~20% of the initial cell volume per second. As our model will predict smaller or similar volume increases, we will assume that water flow is not limiting in the analysis below.

We now suppose that an area A of the cell wall is removed. For simplicity, we assume A to be a circle of radius r_d (Fig. 3 *A*). As discussed in Homogeneity of membrane stresses, we consider bulge geometries with a constant mean curvature. Koiso proved that the only constant mean curvature surfaces with a circular boundary, which are only contained on one side of the boundary, are spherical caps (51). Consistent with the shapes observed in experiments (Figs. 1, *A–C* and 3 *A*), we therefore describe the bulged state by a two-parameter family of geometries in which a spherical bulge, B, of radius R extrudes from A, with the degree of extrusion described by the subtended angle θ (Fig. 3 *A*). At equilibrium, we require that the bulge fills the defect, so that $r_d = R \sin\theta$.

To simplify the analysis and reduce the number of free variables below, we assume the cell wall and the membranes to remain in contact in the cylindrical bulk, so that their strained dimensions are described by the two parameters $r = r^w = r^i = r^o$ and $L = L^w = L^i = L^o$. Relaxing this assumption does not change our results; in particular, repeating the minimization of Eq. 12 below, but allowing (r^w,r^i,r^o) and (L^w,L^i,L^o) to vary independently while satisfying the corresponding steric exclusion constraints, will result in the same minimizers. As the membrane stresses are everywhere equal at equilibrium, the membranes must be in contact in the bulge, so that R and θ do not differ for the IM or OM. The free energy of the bulged state, as denoted by the subscript $_b$, is then

$$\mathcal{F}_b(r_d) = \min_{\substack{r,L,R,r_0^i,L_0^i,r_0^o,L_0^o,\\ R_0^i,R_0^o}} \left[E^i_{\text{stretch}} + E^o_{\text{stretch}}\right](A_B) + \left[E^i_{\text{stretch}} + E^o_{\text{stretch}} + E^w_{\text{stretch}}\right](A_{\text{cell}}) - TS\left(V_b^i\right), \tag{12}$$

where the dependence of the stretching energies on the different geometries are indicated by the areas of the geometries, $A_B = 2\pi R^2(1 - \cos\theta)$ is the strained bulge area, $A = \pi r_d^2$ is the strained area removed, $A_{\text{cell}} = 2\pi rL - A$ is the remaining surface area, ignoring the cellular poles, $S(V_b^i)$ is the entropy of mixing corresponding to an IM volume $V_b^i = \pi r^2 L + V^*$, and $V^* = \pi R^3(2 - 3\cos\theta + \cos^3\theta)/3$ is

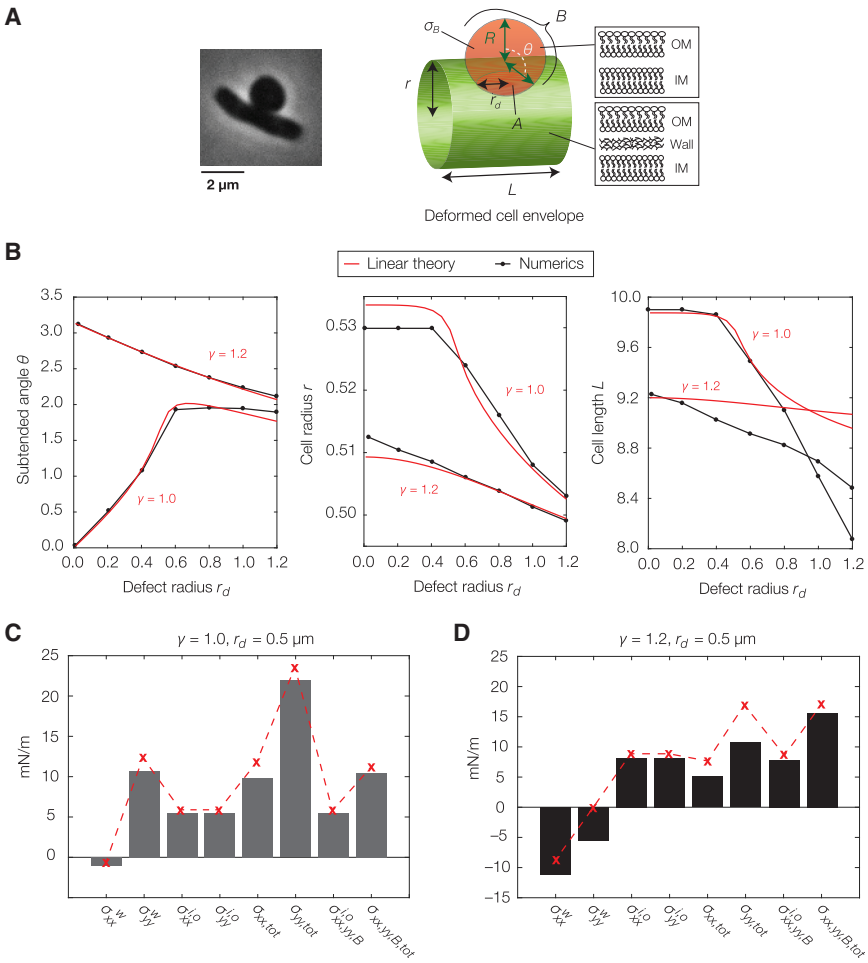

FIGURE 3 Stresses and energetics of the bulged conformation. (*A*) Shown is a schematic of the bulged conformation (*left*), in which a circular cell wall defect of radius r_d is introduced to the strained state and a spherical bulge forms over the defect (*right*). (*B*) Shown are linear theory predictions for the subtended angle (θ), cell radius (r), and cell length (L) as functions of the membrane reference area ratio (γ) and defect radius (r_d) found by solving the bulging equation, Eq. 17. For large defect radii corresponding to large cell wall stresses, the linear theory becomes inaccurate, and the predictions for the cell length deviate. (*C* and *D*) Shown are stresses for the cell wall (w), inner and outer membranes (i and o), and across the entire cell envelope (tot) for $\gamma = 1.0$ and 1.2. The inner and outer membranes are assumed to share identical material properties and exhibit identical stresses. The dashed lines indicate the linear theory predictions found by solving Eq. 17, whereas the bars indicate numerical results. To see this figure in color, go online.

the bulge volume. In the cylindrical bulk, the strained membrane and cell wall dimensions are related to the reference dimensions, r_0 and L_0, in the usual manner by $u_{xx} = (L - L_0)/L_0$ and $u_{yy} = (r - r_0)/r_0$. In the bulge, the strained membrane dimensions are related to the reference membrane dimensions as $u_{xx,B} = u_{yy,B} = (R - R_0)/R$. Accurate to the first order in the strains, the constraint on the reference membrane area for the IM can be expressed as follows:

$$2\pi r_0^i L_0^i - A\left(1 - u_{xx}^i\right)\left(1 - u_{yy}^i\right) + 2\pi\left(R_0^i\right)^2(1 - \cos\theta) \le \mathcal{A}^i, \tag{13}$$

and analogously for the OM. When $\theta = 0$, the cell exhibits no bulging in response to the defect over A.

We proceed to solve for the equilibrium state corresponding to Eq. 12 and the associated reference membrane area constraint both analytically and numerically. The homogeneity of membrane stresses and Laplace's law require the following:

$$\begin{aligned}\sigma_{xx,B}^i &= \sigma_{yy,B}^i = \sigma_{xx,B}^o = \sigma_{yy,B}^o = \sigma_{xx}^i = \sigma_{xx}^o \\ &= \sigma_{yy}^i = \sigma_{yy}^o = \frac{pR}{4},\end{aligned} \tag{14}$$

$$\sigma_{xx}^w + \sigma_{xx}^i + \sigma_{xx}^o = \frac{pr}{2},\ \sigma_{yy}^w + \sigma_{yy}^i + \sigma_{yy}^o = pr,\ p = \frac{kTn_s}{V_b^i}, \tag{15}$$

where $V_b^i = \pi(r_0^w)^2 L_0^w(1 + u_{xx}^w + 2u_{yy}^w) + V^*$, and, as before, all equalities will be accurate to the first order in the strains. Substituting the strain-displacement relations for the cell wall and solving Eqs. 14 and 15, we find the following:

$$\begin{aligned}L &= L_0^w\left(1 + \frac{kTn_s\left(\left(R - 2r_0^w\right)Y_x^w\nu_{yx}^w + \left(r_0^w - R\right)Y_y^w\right)}{2Y_x^wY_y^w\left(\pi(r_0^w)^2L_0^w + V^*\right)}\right), \\ r &= r_0^w\left(1 + \frac{kTn_s\left(Y_x^w\left(2r_0^w - R\right) + \left(R - r_0^w\right)Y_y^w\nu_{xy}^w\right)}{2Y_x^wY_y^w\left(\pi(r_0^w)^2L_0^w + V^*\right)}\right).\end{aligned} \tag{16}$$

Assuming the reference area constraint to be an equality, we note that it uniquely determines the equilibrium state and can be rewritten as $(2\pi rL - \pi r_d^2)(1 - 2u) + (2\pi R^2(1 - \cos\theta))(1 - 2u) = \mathcal{A}^i$, where, at equilibrium, $u = pR/(8K_a)$. As the bulge fills A, $R\sin\theta = r_d$. Combining this

with Eqs. 15 and 16, we re-express the reference area constraint as a single, transcendental equation involving the variable θ only:

$$\mathcal{A}^i = 2\pi r_0^w L_0^w - \pi r_d^2\left(1 - \frac{2}{1+\cos\theta}\right) + \frac{3kTn_s}{4K_a Y_x^w Y_y^w} \times \frac{\Phi(\theta)}{3(r_0^w)^2 L_0^w \sin^3\theta + r_d^3(2+\cos\theta)(\cos\theta-1)^2}, \quad (17)$$

where $\Phi(\theta) = 2r_0^w L_0^w(2K_a r_0^w \sin^3\theta(2Y_x^w(1-\nu_{yx}^w) + Y_y^w(1-\nu_{xy}^w)) - r_d \sin^2\theta(Y_x^w Y_y^w + 2K_a(Y_x^w(1-\nu_{yx}^w) + Y_y^w(1-\nu_{xy}^w))) - r_d^3 Y_x^w Y_y^w \tan^2(\theta/2)\sin^2\theta$. Eq. 17, the bulging equation, is the main result of this work; its solution for θ determines the equilibrium state and all associated variables. Numerical solutions of the bulging equation for different values of r_d and $\mathcal{A}^i$ are shown in Fig. 3 *B*. We find that θ increases with $\mathcal{A}^i$ and that the cell length, and not the radius, predominantly shrinks during bulging. For a typical value of $r_d = 0.5$ μm and $\gamma = 1.0$, these results predict the formation of a hemispherical bulge with $\theta \approx 1.6$ and $R \approx 0.5$ μm, which will be compared with full numerical calculations below.

To gain further intuition for the solutions of the bulging equation, we considered two simple cases. First, asymptotically expanding the bulging equation around $\theta = \pi$, we find the following:

$$\theta \approx \pi - 2r_d\sqrt{\frac{\pi}{\mathcal{A}^i}}, \quad (18)$$

so that, in this limit, large membrane reference areas give rise to full and large bulges, irrespective of the material properties of the cell envelope. Indeed, for full bulges, Eq. 18 shows that the subtended angle depends only on the ratio of defect to reference areas, $A/\mathcal{A}^i$. Second, we considered a simple case in which $Y_x^w = Y_y^w = Y$ and neglected Poisson's effect. Accurate to the first order in r_d/R, the solution of the bulging equation reduces to the following:

$$\theta \approx \frac{r_d}{R}, \quad R \approx \frac{6kTn_s K_a r_0^w - 4(\gamma-1)K_a Y\pi(r_0^w)^2 L_0^w}{kTn_s(4K_a+Y)}. \quad (19)$$

Thus, our model predicts that, for small cell wall defects relative to the bulge radius, cells with large membrane reference areas produce full, but small, bulges, whereas cells with small membrane reference areas produce shallow, but large, ones. These results are consistent with Fig. 3 *B* and the intuition that cells with excess membrane area may form large bulges by "throwing away" the excess area. Nevertheless, a comparison to experimental data will suggest the excess membrane area in typical cells to lie in a limited range (see Model of swelling below).

To support the analytical calculations above, we numerically computed the minimum of Eq. 12 over the 9 independent variables subject to the reference area constraint. We found that, for a range of $\mathcal{A}^i$, the numerical minimizers of Eq. 12 are generally well described by the linear theory (Fig. 3, *B–D*; Table S1). When $r_d = 0.5$ μm and $\gamma = 1.0$, for instance, we find that $\theta \approx 1.5$ and $R \approx 0.5$ μm, in excellent agreement with the linear theory. These results also predict that the cell length, in contrast to the cell width, shrinks significantly during bulging (Fig. 3 *B*). Consistent with our assumption that water flow is not limiting during bulging, when $r_d = 0.5$ μm and $\gamma = 1.0$, the fractional volume increase relative to the healthy state is $\Delta V < 1\%$, whereas for $\gamma = 1.2$, ΔV increases to $\Delta V \approx 25\%$. As mentioned above, typical values of L_p for bacteria predict volume increases on the order of $\Delta V \approx 20\%$ per second. Thus, we conclude that bulging is energetically favorable, and the observed timescale of bulging is consistent with water flow into the membrane.

Implications for dynamics

The foregoing analyses show that, for a range of membrane reference areas, bulging corresponds to an equilibrium state: the only stable configuration of the cellular envelope is one in which bulging occurs. In general, our model predicts that partially subtended, spherical bulges form upon the introduction of cell wall defects (Fig. 3 *B*) and clarify the resulting stresses (Fig. 3, *C* and *D*). By elucidating the factors determining bulge size, our results reveal the importance of membrane stretching and contrast with Daly et al.'s study examining critical defect sizes for bulge nucleation (28), in which the authors studied the trade-off between the bending energy cost of bulging and the pressure-volume energy gained.

Our model also assumes that the membranes may slide against the wall because of the differing strain rates of envelope components. For instance, u_{xx}^w typically decreases after bulging, whereas u_{xx}^i and u_{xx}^o remain approximately unchanged (Figs. 2, *B* and *C* and 3, *C* and *D*). Although molecules such as Braun's lipoprotein anchor the OM to the cell wall, the estimated number of such OM-wall anchors ($\sim 10^6$) are few in comparison to the estimated numbers ($\sim 10^7$) of phospholipids (52,53). Hence, free phospholipids could modulate the reference states and allow for membrane reorganization. The assumption of sliding is therefore consistent with physical coupling of the OM to the cell wall.

Importantly, a central prediction of our model is that bulging arises as a relaxation process. Hence, the timescale of bulging is determined by the equilibration of $\mathcal{F}_b$. Balancing the energy dissipation with the viscous drag on the bulge results in a timescale much smaller than 100 ms (Supporting Materials and Methods), suggesting that the relaxation time may specifically be limited by membrane reorganization (54). We anticipate further experiments

(for instance, ones that modulate membrane fluidity during β-lactam killing) to better clarify the processes limiting relaxation.

Model of swelling

Having shown that bulging arises as a relaxation process leading to a metastable state, we now demonstrate that swelling—the increase of bulge volume over a much longer timescale of minutes—is consistent with the growth of cell wall defects. As we anticipate that the energetic trade-offs considered above remain relevant on the slower timescale in which cell wall defects grow, the model of bulging also predicts bulge size during swelling, as shown below. The significant difference between the timescales of bulging and swelling (Fig. 1 *D*) can then be explained by a separation of timescales due to 1) energetic relaxation and 2) defect growth.

During swelling, the amount of water uptake is determined by the same balance of the entropic and stretching energies of the cellular envelope as above; if lysis did not occur, then net flow into the cytoplasm would occur until the membranes are sufficiently stretched. In fact, the small synthesis rate of membrane material relative to water flow (41) suggests that water flow is not limiting and that the membranes are always stretched. To support this notion, we analyzed the swelling of *E. coli* cells of different lengths over ~10 s and found that the population-averaged volumetric flow rate does not depend on the membrane surface area (Fig. 4 *A*), as would be the case if membrane synthesis was fast and water flow became limiting. In contrast, image analysis reveals that bulges grow at a rate consistent with Eq. 12 when the defect radius, r_d, also increases, supporting the notion that the reference membrane areas remain limiting (Fig. 4 *B*). This result therefore suggests defect growth to be the limiting step of bulge growth before lysis.

We next wondered whether the observed range of bulge volumes suggested a typical value for the excess membrane area; indeed, we found that the empirically observed fractional bulge volumes in Fig. 4 *B* suggest any pre-existing excess membrane area in healthy cells to be limited. In the case in which $\gamma = 1.5$, for instance, the formation of a full bulge of radius $R \approx 1$ μm, corresponding to a fractional bulge volume of $V^*/V_b^i \approx 0.4$, would be energetically favorable even for limitingly small defect radii as the cell initially "throws away" the excess membrane area. Nevertheless, as shown in Fig. 4 *B*, such large bulge volumes are not observed for defect radii less than ~0.8 μm. Instead, the data are consistent with excess membrane area in the range of $\gamma = 1.0$ to $\gamma = 1.2$, and the value $\gamma = 1.05$ provides the best fit (Fig. 4 *B*). Intriguingly, the solution of Eq. 17 predicts a sharp increase in bulge volume when $\gamma = 1.05$ and $r_d \approx 0.3$ μm, which arises from the transition between small and large subtended angles (Fig. 3 *B*). For larger values of γ such as $\gamma = 1.2$, the subtended angles are large across a broader range of r_d (Fig. 3 *B*), and hence, the predicted dependence of bulge volume on the defect radius becomes much shallower.

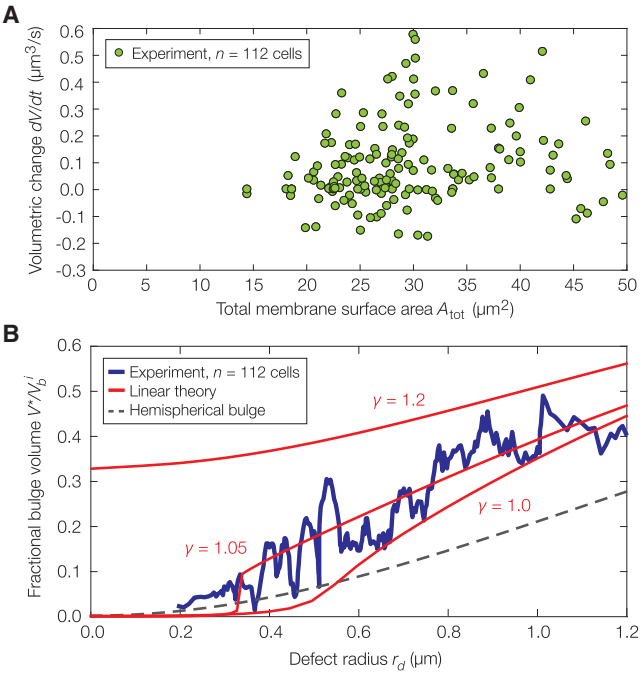

FIGURE 4 Statistics of swelling cells. (*A*) Shown is a plot of the volumetric flow rate dV/dt against the total membrane surface area A_{tot} for 112 swelling cells of different lengths and one or two data points per cell. Bulged cells were fit to cylinders with protruding spheres; see the Supporting Materials and Methods for details on the image analysis methodology. The scatter indicates cell-to-cell variability. As the slope of a linear fit to the data is $(2 \pm 5) \times 10^{-9}$ m^3·Pa/N·s, dV/dt does not increase with A_{tot} as $dV/dt = L_p A_{tot} p$, and we conclude that the cellular volume increase during swelling is not governed by water flow. (*B*) Shown is a plot of the moving average of V^*/V_b^i, the fractional bulge volume, against the defect radius r_d for the same cells in (*A*), with 1) the linear theory predictions for different γ, as found by solving Eq. 17, and 2) the prediction corresponding to adding a hemispherical bulge of radius r_d irrespective of the model overlaid. To see this figure in color, go online.

As our model also predicts that the mechanical stresses in the bulge increase because of increasing bulge size, swelling may occur until the cell lyses. Since the mean bulge radius at lysis is $R \approx 0.8$ μm, assuming the same parameter values as in Materials and Methods and that the number of solutes has not changed due to osmotic stress responses (45–47,49,55–57) suggests the yield areal strain of the *E. coli* IM and OM to be approximately 20%. This estimate is consistent with the empirical range of RBCs and lipid vesicles that are stretched on the timescale of 0.1–100 s (58–60) and exceeds that of RBCs under quasistatic loading (61). The final step of lysis is, therefore, consistent with material failure of the IM and OM under turgor pressure loading.

CONCLUSIONS

To summarize, we have used a continuum, elastic description of the cellular envelope to model membrane bulging and found evidence that defect enlargement underlies swelling. Our results underscore the different roles of each envelope component in resisting mechanical stresses and indicate that bulging can arise as a relaxation process mediated by membrane fluidity and water flow once a wall defect exists. These findings have implications on cellular physiology and morphogenesis. Because bulging and swelling result in eventual lysis and are mediated by cell wall defects, the existence of large pores in bacterial cell walls can be deadly.

In many rod-shaped bacteria, including *E. coli*, the cell wall is locally and dynamically remodeled by protein complexes that rotate around the cell, but how these protein complexes maintain a cell-spanning rod shape is unknown (62–66). Our work shows that cell wall remodeling processes must regulate pore size and suggests constraints on how PG synthases can hydrolyze preexisting PG. Although cell wall remodeling at the scale of the micron-sized defects considered here occurs on a slower timescale than that of bulging (22), a growth mechanism that regulates pore size could preemptively help cells avoid lysis, in addition to regulating wall thickness and straight, rod-like morphology (33). In general, our work illustrates that analyzing mechanical instabilities and failure modes in cells can constrain how physiological growth pathways function. Conversely, exploiting the physical consequences of large cell wall defects may lead to novel approaches for developing new antibiotics.

Beyond bacterial morphogenesis, the combination of theory and experiment in our work has underscored characteristics of biological membrane physics and the importance of mechanical stresses in cells. By being free to change their reference geometries, fluid membranes differ from rigid, elastic shells, and we have shown that this difference has physiological implications on cell envelope mechanics and how mechanical stresses are distributed between membrane-solid layers. Our study therefore paves the way for investigating similar interactions of fluid membranes with elastic surfaces (67) and understanding the material nature of living cells across different contexts.

SUPPORTING MATERIAL

Supporting Material can be found online at https://doi.org/10.1016/j.bpj.2019.04.040.

AUTHOR CONTRIBUTIONS

F.W. and A.A. conceived the project, performed modeling, and wrote the article. F.W. performed experiments and analyzed data.

ACKNOWLEDGMENTS

We thank John W. Hutchinson, Michael Moshe, and Yohai Bar-Sinai for numerous extended discussions, Kranthi K. Mandadapu, Amaresh Sahu, John W. Hutchinson, L. Mahadevan, Shmuel M. Rubinstein, Haim Diamant, Roy Kishony, Ugur Çetiner, and Zhizhong Yao for helpful feedback, Ethan C. Garner, Sean Wilson, and Georgia Squyres for microscopy assistance, Thomas G. Bernhardt and Sue Sim for the BW25113 strain, and Michael Moshe, Po-Yi Ho, and Jie Lin for comments on the manuscript. We gratefully thank the anonymous reviewers for their important feedback.

F.W. was supported by the National Science Foundation Graduate Research Fellowship under grant DGE1144152 and the Quantitative Biology Initiative at Harvard. A.A. was supported by the Alfred P. Sloan Foundation and the Volkswagen Foundation. Both authors were supported by the Materials Research and Engineering Center at Harvard University under grant DMR-1420570 and the Kavli Institute for Bionano Science and Technology at Harvard University.

SUPPORTING CITATIONS

References (68,69) appear in the Supporting Material.

REFERENCES

1. World Health Organization. 2014. Antimicrobial Resistance: Global Report on Surveillance. WHO, Geneva, Switzerland.
2. Ventola, C. L. 2015. The antibiotic resistance crisis: part 1: causes and threats. *P&T.* 40:277–283.
3. Bao, G., and S. Suresh. 2003. Cell and molecular mechanics of biological materials. *Nat. Mater.* 2:715–725.
4. Guillot, C., and T. Lecuit. 2013. Mechanics of epithelial tissue homeostasis and morphogenesis. *Science.* 340:1185–1189.
5. Ladoux, B., and R. M. Mège. 2017. Mechanobiology of collective cell behaviours. *Nat. Rev. Mol. Cell Biol.* 18:743–757.
6. Lederberg, J. 1957. Mechanism of action of penicillin. *J. Bacteriol.* 73:144.
7. Ciak, J., and F. E. Hahn. 1957. Penicillin-induced lysis of *Escherichia coli*. *Science.* 125:119–120.
8. Benveniste, R., and J. Davies. 1973. Mechanisms of antibiotic resistance in bacteria. *Annu. Rev. Biochem.* 42:471–506.
9. Tomasz, A. 1979. The mechanism of the irreversible antimicrobial effects of penicillins: how the beta-lactam antibiotics kill and lyse bacteria. *Annu. Rev. Microbiol.* 33:113–137.
10. Kohanski, M. A., D. J. Dwyer, …, J. J. Collins. 2007. A common mechanism of cellular death induced by bactericidal antibiotics. *Cell.* 130:797–810.
11. Kohanski, M. A., D. J. Dwyer, and J. J. Collins. 2010. How antibiotics kill bacteria: from targets to networks. *Nat. Rev. Microbiol.* 8:423–435.
12. Cho, H., T. Uehara, and T. G. Bernhardt. 2014. Beta-lactam antibiotics induce a lethal malfunctioning of the bacterial cell wall synthesis machinery. *Cell.* 159:1300–1311.
13. Höltje, J. V. 1998. Growth of the stress-bearing and shape-maintaining murein sacculus of *Escherichia coli*. *Microbiol. Mol. Biol. Rev.* 62:181–203.
14. Amir, A., and S. van Teeffelen. 2014. Getting into shape: how do rod-like bacteria control their geometry? *Syst. Synth. Biol.* 8:227–235.
15. Young, K. D. 2006. The selective value of bacterial shape. *Microbiol. Mol. Biol. Rev.* 70:660–703.
16. Yao, Z., D. Kahne, and R. Kishony. 2012. Distinct single-cell morphological dynamics under beta-lactam antibiotics. *Mol. Cell.* 48:705–712.
17. Koch, A. L. 2001. Bacterial Growth and Form. Springer Science & Business Media, New York.

18. Chung, H. S., Z. Yao, …, D. Kahne. 2009. Rapid β-lactam-induced lysis requires successful assembly of the cell division machinery. *Proc. Natl. Acad. Sci. USA.* 106:21872–21877.
19. Huang, K. C., R. Mukhopadhyay, …, N. S. Wingreen. 2008. Cell shape and cell-wall organization in Gram-negative bacteria. *Proc. Natl. Acad. Sci. USA.* 105:19282–19287.
20. Cushnie, T. P., N. H. O'Driscoll, and A. J. Lamb. 2016. Morphological and ultrastructural changes in bacterial cells as an indicator of antibacterial mechanism of action. *Cell. Mol. Life Sci.* 73:4471–4492.
21. Deng, Y., M. Sun, and J. W. Shaevitz. 2011. Direct measurement of cell wall stress stiffening and turgor pressure in live bacterial cells. *Phys. Rev. Lett.* 107:158101.
22. Amir, A., F. Babaeipour, …, S. Jun. 2014. Bending forces plastically deform growing bacterial cell walls. *Proc. Natl. Acad. Sci. USA.* 111:5778–5783.
23. Yao, X., M. Jericho, …, T. Beveridge. 1999. Thickness and elasticity of Gram-negative murein sacculi measured by atomic force microscopy. *J. Bacteriol.* 181:6865–6875.
24. Lan, G., C. W. Wolgemuth, and S. X. Sun. 2007. Z-ring force and cell shape during division in rod-like bacteria. *Proc. Natl. Acad. Sci. USA.* 104:16110–16115.
25. Sun, Y., T. L. Sun, and H. W. Huang. 2014. Physical properties of *Escherichia coli* spheroplast membranes. *Biophys. J.* 107:2082–2090.
26. Boal, D. 2002. Mechanics of the Cell. Cambridge University Press, Cambridge, UK.
27. Phillips, R., J. Kondev, …, H. Garcia. 2012. Physical Biology of the Cell. Garland Science, New York.
28. Daly, K. E., K. C. Huang, …, R. Mukhopadhyay. 2011. Mechanics of membrane bulging during cell-wall disruption in Gram-negative bacteria. *Phys. Rev. E Stat. Nonlin. Soft Matter Phys.* 83:041922.
29. Safran, S. A. 2003. Statistical Thermodynamics of Surfaces, Interfaces, and Membranes. Westview Press, Boulder, CO.
30. Behroozi, F. 1996. Theory of elasticity in two dimensions and its applications to Langmuir-Blodgett films. *Langmuir.* 12:2289–2291.
31. Bermúdez, H., D. A. Hammer, and D. E. Discher. 2004. Effect of bilayer thickness on membrane bending rigidity. *Langmuir.* 20:540–543.
32. Waugh, R., and E. A. Evans. 1979. Thermoelasticity of red blood cell membrane. *Biophys. J.* 26:115–131.
33. Wong, F., L. D. Renner, …, A. Amir. 2017. Mechanical strain sensing implicated in cell shape recovery in *Escherichia coli*. *Nat. Microbiol.* 2:17115.
34. Calladine, C. R. 1983. Theory of Shell Structures. Cambridge University Press, Cambridge, UK.
35. Santangelo, C. D. 2009. Buckling thin disks and ribbons with non-Euclidean metrics. *EPL.* 86:34003.
36. Evans, E. A., and R. Waugh. 1977. Osmotic correction to elastic area compressibility measurements on red cell membrane. *Biophys. J.* 20:307–313.
37. Kwok, R., and E. Evans. 1981. Thermoelasticity of large lecithin bilayer vesicles. *Biophys. J.* 35:637–652.
38. Diz-Muñoz, A., D. A. Fletcher, and O. D. Weiner. 2013. Use the force: membrane tension as an organizer of cell shape and motility. *Trends Cell Biol.* 23:47–53.
39. Dai, J., and M. P. Sheetz. 1999. Membrane tether formation from blebbing cells. *Biophys. J.* 77:3363–3370.
40. Sheetz, M. P. 2001. Cell control by membrane-cytoskeleton adhesion. *Nat. Rev. Mol. Cell Biol.* 2:392–396.
41. Bendezú, F. O., and P. A. de Boer. 2008. Conditional lethality, division defects, membrane involution, and endocytosis in *mre* and *mrd* shape mutants of *Escherichia coli*. *J. Bacteriol.* 190:1792–1811.
42. Billings, G., N. Ouzounov, …, K. C. Huang. 2014. *De novo* morphogenesis in L-forms via geometric control of cell growth. *Mol. Microbiol.* 93:883–896.
43. Hwang, H., N. Paracini, …, J. C. Gumbart. 2018. Distribution of mechanical stress in the *Escherichia coli* cell envelope. *Biochim Biophys Acta Biomembr.* 1860:2566–2575.
44. Rojas, E. R., G. Billings, …, K. C. Huang. 2018. The outer membrane is an essential load-bearing element in Gram-negative bacteria. *Nature.* 559:617–621.
45. Buda, R., Y. Liu, …, T. Pilizota. 2016. Dynamics of *Escherichia coli*'s passive response to a sudden decrease in external osmolarity. *Proc. Natl. Acad. Sci. USA.* 113:E5838–E5846.
46. Pilizota, T., and J. W. Shaevitz. 2012. Fast, multiphase volume adaptation to hyperosmotic shock by *Escherichia coli*. *PLoS One.* 7:e35205.
47. Rojas, E., J. A. Theriot, and K. C. Huang. 2014. Response of *Escherichia coli* growth rate to osmotic shock. *Proc. Natl. Acad. Sci. USA.* 111:7807–7812.
48. Sperelakis, N. 1995. Cell Physiology Source Book: Essentials of Membrane Biophysics. Academic Press, Cambridge, MA.
49. Çetiner, U., I. Rowe, …, S. Sukharev. 2017. Tension-activated channels in the mechanism of osmotic fitness in *Pseudomonas aeruginosa*. *J. Gen. Physiol.* 149:595–609.
50. Peterlin, P., V. Arrigler, …, H. Diamant. 2012. Law of corresponding states for osmotic swelling of vesicles. *Soft Matter.* 8:2185–2193.
51. Koiso, M. 1986. Symmetry of hypersurfaces of constant mean curvature with symmetric boundary. *Math. Z.* 191:567–574.
52. Silhavy, T. J., D. Kahne, and S. Walker. 2010. The bacterial cell envelope. *Cold Spring Harb. Perspect. Biol.* 2:a000414.
53. Movva, N. R., K. Nakamura, and M. Inouye. 1980. Regulatory region of the gene for the ompA protein, a major outer membrane protein of *Escherichia coli*. *Proc. Natl. Acad. Sci. USA.* 77:3845–3849.
54. Evans, E. A., and R. M. Hochmuth. 1976. Membrane viscoelasticity. *Biophys. J.* 16:1–11.
55. Reuter, M., N. J. Hayward, …, I. R. Booth. 2013. Mechanosensitive channels and bacterial cell wall integrity: does life end with a bang or a whimper? *J. R. Soc. Interface.* 11:20130850.
56. Bialecka-Fornal, M., H. J. Lee, and R. Phillips. 2015. The rate of osmotic downshock determines the survival probability of bacterial mechanosensitive channel mutants. *J. Bacteriol.* 197:231–237.
57. Boer, M., A. Anishkin, and S. Sukharev. 2011. Adaptive MscS gating in the osmotic permeability response in *E. coli*: the question of time. *Biochemistry.* 50:4087–4096.
58. Li, F., C. U. Chan, and C. D. Ohl. 2013. Yield strength of human erythrocyte membranes to impulsive stretching. *Biophys. J.* 105:872–879.
59. Rand, R. P. 1964. Mechanical properties of the red cell membrane. II. Viscoelastic breakdown of the membrane. *Biophys. J.* 4:303–316.
60. Chabanon, M., J. C. S. Ho, …, P. Rangamani. 2017. Pulsatile lipid vesicles under osmotic stress. *Biophys. J.* 112:1682–1691.
61. Evans, E. A., R. Waugh, and L. Melnik. 1976. Elastic area compressibility modulus of red cell membrane. *Biophys. J.* 16:585–595.
62. Garner, E. C., R. Bernard, …, T. Mitchison. 2011. Coupled, circumferential motions of the cell wall synthesis machinery and MreB filaments in *B. subtilis*. *Science.* 333:222–225.
63. Domínguez-Escobar, J., A. Chastanet, …, R. Carballido-López. 2011. Processive movement of MreB-associated cell wall biosynthetic complexes in bacteria. *Science.* 333:225–228.
64. van Teeffelen, S., S. Wang, …, Z. Gitai. 2011. The bacterial actin MreB rotates, and rotation depends on cell-wall assembly. *Proc. Natl. Acad. Sci. USA.* 108:15822–15827.
65. Hussain, S., C. N. Wivagg, …, E. C. Garner. 2018. MreB filaments align along greatest principal membrane curvature to orient cell wall synthesis. *eLife.* 7:e32471.
66. Wong, F., E. C. Garner, and A. Amir. 2019. Mechanics and dynamics of translocating MreB filaments on curved membranes. *eLife.* 8:e40472.
67. Staykova, M., D. P. Holmes, …, H. A. Stone. 2011. Mechanics of surface area regulation in cells examined with confined lipid membranes. *Proc. Natl. Acad. Sci. USA.* 108:9084–9088.

68. Ventsel, E., and T. Krauthammer. 2001. Thin Plates and Shells: Theory, Analysis, and Applications. Marcel Dekker, Inc., New York.

69. Spurk, J. H. 1997. Fluid Mechanics: Problems and Solutions. Springer-Verlag, New York.

70. Gan, L., S. Chen, and G. J. Jensen. 2008. Molecular organization of Gram-negative peptidoglycan. *Proc. Natl. Acad. Sci. USA.* 105:18953–18957.

71. Koch, A. L. 1990. Additional arguments for the key role of "smart" autolysins in the enlargement of the wall of Gram-negative bacteria. *Res. Microbiol.* 141:529–541.

72. Cayley, D. S., H. J. Guttman, and M. T. Record, Jr. 2000. Biophysical characterization of changes in amounts and activity of *Escherichia coli* cell and compartment water and turgor pressure in response to osmotic stress. *Biophys. J.* 78:1748–1764.

Biophysical Journal, Volume *116*

Supplemental Information

Mechanics and Dynamics of Bacterial Cell Lysis

Felix Wong and Ariel Amir

Guide to the SM

For the convenience of readers, here we summarize main text references to the SM and note which SM sections correspond to which references.

1. *The Supporting Material contains further details regarding bacterial growth, microscopy, and image analysis.*

   See *Supporting Materials and Methods*.

2. *We therefore discard the bending energies in the expressions below and verify in the Supporting Material that they do not change our results.*

   See *Bending energies are negligible*.

3. *Balancing the energy dissipation with the viscous drag on the bulge results in a timescale much smaller than 100 ms (Supporting Material), suggesting that the relaxation time may specifically be limited by water flow or membrane reorganization.*

   See *Timescale of the bulging response against viscous drag*.

4. *Bulged cells were fit to cylinders with protruding spheres; see the Supporting Material for details on the image analysis methodology.*

   See *Supporting Materials and Methods*.

Supporting Materials and Methods

Bacterial strains and growth

The wild-type strain used in this study is *E. coli* MG1655, and we verified that the morphological dynamics is statistically indistinguishable in two other wild-type strains, JOE309 and BW25113. Cells were grown in liquid LB (LB: 10 g/L tryptone, 5 g/L yeast extract, 10 g/L NaCl) supplemented with no antibiotics. LB media containing 1.5% Difco agar (w/v) was used to grow individual colonies. Cells were taken from an overnight culture, diluted 100-fold, and grown in LB at 37°C in a roller drum agitating at 60 rpm to an absorbance of approximately 0.3 to 0.6 ($\lambda = 600$ nm). Cells were then concentrated by centrifugation at 3000 rpm for 5 min and resuspended. We added 1 μL of the bacterial culture to No. 1.5 coverslips (24×60 mm) and placed on top a 1 mm thick LB agarose (1.5%) pad containing 50 μg/mL of cephalexin, a β-lactam antibiotic, for imaging. Cephalexin was made fresh before each experiment, and cells were imaged immediately after placing the pad.

Microscopy

We used a Nikon Ti inverted microscope (Nikon, Tokyo, Japan) equipped with a 6.5 μm-pixel Hamamatsu CMOS camera (Hamamatsu, Hamamatsu City, Japan) and a Nikon 100x NA 1.45 objective (Nikon, Tokyo, Japan) for imaging. All cells were imaged at 37°C on a heated stage. The time between each frame during timelapse measurements ranged from 10 ms to 2 s, and the duration of timelapses varied from 10 min to 3 h. Images were recorded using NIS-Elements software (Nikon, Tokyo, Japan).

Image analysis

Timelapses were compiled from previous work [1] and from ten replicate experiments described above, which resulted in raw data for over 500 cells. Frames were annotated manually in ImageJ (National Institutes of Health, Bethesda, MD). Bulged cells were fit to cylinders with protruding spheres with radii R, as shown in Fig. 3A of the main text, to determine cellular dimensions, bulge radii, defect radii, and subtended bulge angles. All cells considered bulged in the imaging plane. For Fig. 1D of the main text, a subset of 176 cells were chosen as cells for which bulging and lysis could be clearly resolved. For Fig. 4 of the main text, a subset of 112 cells were chosen as cells which bulged on a timescale $\sim$1 s, for which the cellular dimensions

could be determined, and for which the relevant statistics could be measured or computed at two or three time points until ∼10 seconds after bulging. This choice of timescale was made to mitigate the potential influence of cellular stress responses such as transport of solutes out of the cytoplasm [2], which could confound volumetric measurements. We applied a trailing moving average filter of 10 points to generate the moving average curve in Fig. 4B of the main text.

Bending energies are negligible

Throughout this work, we have assumed that the bending energies are negligible compared to the stretching energies. The bending energy of an isotropic shell is $E_{\text{bend}} = 2k_b \int H^2 dA$. Here k_b is the bending rigidity, H is the mean curvature, a vanishing spontaneous curvature is assumed for all surfaces for simplicity, and the contribution of Gaussian curvature to the elastic energy is ignored due to the Gauss-Bonnet theorem and absence of topological change. The bending energy E^w_{bend} of the orthotropic cell wall assumes a more complicated form involving bending rigidities in the xx, xy, and yy directions [3]. However, here we do not consider bending deformations of the cell wall. We therefore leave the form of E^w_{bend} unspecified and ignore it in the following. We now consider the addition of these bending energies to the analysis in this study.

Here and below, we assume $r = r^i = r^o$ and $L = L^i = L^o$, which is consistent with the energetic minimum found in the main text, but note that substantial variation in r and L do not significantly change the following results. The combined bending energy of the bulged state, corresponding to Eq. (12) in the main text, is

$$\mathcal{E}_1 = \frac{A_{\text{cell},b}(k_b^i + k_b^o)}{2r^2} + 4\pi(k_b^i + k_b^o)(1 - \cos\theta) + \mathcal{E}_{\text{neck}}, \tag{S1}$$

where $A_{\text{cell},b} = 2\pi rL - A$ and $\mathcal{E}_{\text{neck}}$ is the bending energy of the bulge neck, which we now estimate. For a spherical bulge joined to a cylinder, the mean curvature diverges at the kink of the neck. In lieu of a perfect kink, we may suppose instead that the geometry of the neck is described by a partial, circular torus of major and minor radii D and C (Fig. S1). While such a geometry cannot generally exist at equilibrium due to the discussion in *Homogeneity of membrane stresses*, it will be helpful for estimating the strain energy.

For the torus, C can be set to satisfy conservation of membrane reference surface areas, so that the reference area of the torus is identical to the reference area of the neck that it replaces; however, D is constrained by the bulge radius to be $D \approx R\sin\theta$. For cases in which the subtended angle $\theta \leq \pi/2$, the sector of the toroidal cross-section needed to bridge the neck can be taken to be $\leq \theta$ with its value dependent on the choice of C, while for $\theta > \pi/2$, half of the cross-section suffices over a range of C (Fig. S1). Then, as the area of the toroidal neck is bounded by $A_{\text{neck}} \lesssim (\frac{\theta}{2\pi}) \times 4\pi^2 CD$, the bending energy of the toroidal neck satisfies

$$\mathcal{E}_{\text{neck}} \lesssim \begin{cases} \theta\pi CDk_b \left(\frac{1}{C} + \frac{1}{D-C}\right)^2 & \theta \leq \pi/2 \\ \frac{\pi^2 CDk_b}{2} \left(\frac{1}{C} + \frac{1}{D-C}\right)^2 & \theta > \pi/2. \end{cases} \tag{S2}$$

For $k_b = 20\ kT$, $D \sim 1\ \mu$m, and $C \sim 10$ nm, we find that the bending energy corrections indicated in equation (S1) are of a lower order of magnitude ($\sim 10^{-17}$ J) than the energy scale considered in the main text ($\sim 10^{-14}$ J, as shown in Table S1). Note that, while the stretching energy may also increase if the bulge neck is stretched, for characteristic values of $D \sim 1\ \mu$m and $C \sim 10$ nm the reference surface area occupied by the bulge neck is on the order of 1% of that of the bulge. For simplicity, we may therefore suppose the bulge neck to be unstrained without significantly changing any of the results presented in the main text. Taken together, these considerations suggest that it is indeed justifiable to neglect the bending energies and the energetic contribution of the neck; neither do they present energetic barriers to relaxation.

Timescale of the bulging response against viscous drag

We show that balancing the energy change computed above with the viscous drag on the bulge implies a timescale that is smaller than 100 ms, and hence energy dissipation cannot account for the observed timescale of bulging. The characteristic scale of the free energy change due to bulging in our work is 10^{-14} J, while the power dissipation due to viscous drag on an expanding sphere is $16\pi\eta\dot{R}^2R$, where η denotes the medium viscosity and R is the radius of the sphere [4]. Supposing the viscosity of water, $\eta = 10^{-3}$ Pa$\cdot$s, and estimating $R = 0.5$ μm and $\dot{R} = 0.5$ μm$/(100$ ms$)$ then results in an energy scale of 10^{-19} J/s. Equivalently, a power dissipation of 10^{-14} J$/(100$ ms$)$ implies a bulging timescale of ~ 0.1 ms.

Supporting Movies

Movie S1: **Lysis dynamics of *E. coli* cells.** Movie S1 shows a population of wild-type *E. coli* cells bulging, swelling, and lysing under antibiotic treatment. The time between frames is 30 seconds, the timelapse covers a period of approximately 1 hour, and the field of view is 100 μm $\times$ 80 μm.

Supporting References

[1] Yao, Z., Kahne, D. & Kishony, R. Distinct single-cell morphological dynamics under beta-lactam antibiotics. *Mol. Cell* **48**, 705–712 (2012).

[2] Buda, R. *et al.* Dynamics of *Escherichia coli*'s passive response to a sudden decrease in external osmolarity. *Proc. Natl. Acad. Sci. USA* **113**, E5838–E5846 (2016).

[3] Ventsel, E. & Krauthammer, T. *Thin Plates and Shells: Theory, Analysis, and Applications* (Marcel Dekker, Inc., 2001).

[4] Spurk, J. H. *Fluid Mechanics: Problems and Solutions* (Springer-Verlag, 1997).

γ	1.0	1.2
Eq. (7) in the main text		
r^w	0.530 (0.534)	0.539 (0.552)
L^w	9.989 (9.875)	10.555 (10.875)
r^i	0.530 (0.534)	0.539 (0.552)
L^i	9.989 (9.875)	10.555 (10.875)
r^o	0.530 (0.534)	0.539 (0.552)
L^o	9.989 (9.875)	10.555 (10.875)
r_0^i	0.517 (0.519)	0.539 (0.555)
L_0^i	9.673 (9.604)	10.555 (10.917)
r_0^o	0.517 (0.519)	0.539 (0.555)
L_0^o	9.673 (9.604)	10.555 (10.917)
$\mathcal{F}_e$	-3.5307e-12 (-3.5299e-12)	-3.5528e-12 (-3.5442e-12)
Eq. (12) in the main text		
r	0.529 (0.530)	0.509 (0.507)
L	9.780 (9.758)	8.940 (9.163)
r_0^i	0.516 (0.516)	0.489 (0.485)
L_0^i	9.520 (9.488)	8.585 (8.775)
r_0^o	0.516 (0.516)	0.489 (0.485)
L_0^o	9.520 (9.488)	8.585 (8.775)
R_0^i	0.491 (0.486)	1.010 (0.998)
R_0^o	0.491 (0.486)	1.010 (0.998)
R	0.504 (0.500)	1.049 (1.042)
θ	1.445 (1.587)	2.645 (2.641)
$\mathcal{F}_b$	-3.5342e-12 (-3.5357e-12)	-3.6354e-12 (-3.6389e-12)

Table S1: Approximate minimizers (in units of μm or J) found numerically for different values of γ and, for Eq. (12) in the main text, $r_d = 0.5$ μm. For comparison, the linear theory estimates are shown in parentheses.

Supporting Figures

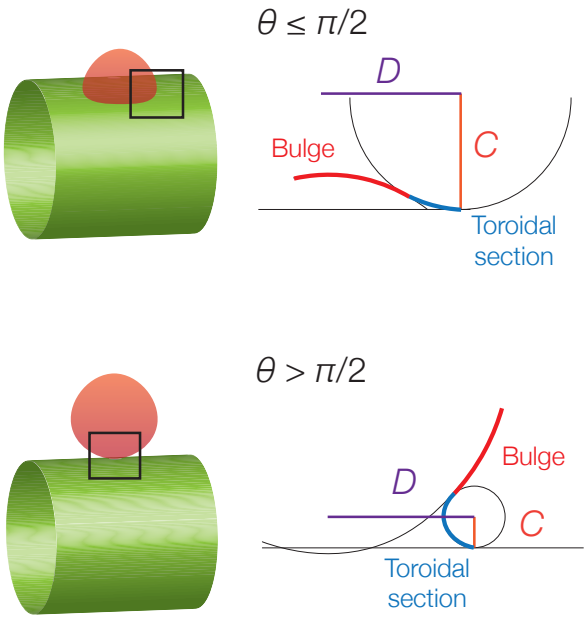

Figure S1: **Bending energy at the neck.** To avoid the divergence of the bending energy at the neck, we connect the bulge to the cylindrical bulk with a partial torus and estimate the resulting energetic contribution. The planar diagrams show cross-sections of the axisymmetric geometries.